

NUMERICAL INTEGRATION OF THE PRIMITIVE EQUATIONS WITH A FLOATING SET OF COMPUTATION POINTS: EXPERIMENTS WITH A BAROTROPIC GLOBAL MODEL¹

FEDOR MESINGER²

Department of Meteorology, University of California, Los Angeles, Calif.

ABSTRACT

A Lagrangean-type numerical forecasting method is developed in which the computational (grid) points are advected by the wind and the necessary space derivatives (in the pressure gradient terms, for example) are computed using the values of the variables at all the computation points that at the particular moment are within a prescribed distance of the point for which the computation is done. In this way, the forecasting problem reduces to solving the ordinary differential equations of motion and thermodynamics for each computation point, instead of solving the partial differential equations in the Eulerian or classical Lagrangean way. The method has some advantages over the conventional Eulerian scheme: simplicity (there are no advection terms), lack of computational dispersion in the advection terms and therefore better simulation of atmospheric advection and deformation effects, very little inconvenience due to the spherical shape of the earth, and the possibility for a variable space resolution if desired. On the other hand, some artificial smoothing may be necessary, and it may be difficult (or impossible) to conserve the global integrals of certain quantities.

A more detailed discussion of the differencing scheme used for the time integration is included in a separate section. This is the scheme obtained by linear extrapolation of computed time derivatives to a time value of $t_0 + \alpha \Delta t$ where t_0 is the value of time at the beginning of the considered time step Δt and where α is a parameter that can be used to control the properties of the scheme. When choosing a value of α between $\frac{1}{2}$ and 1, a scheme is obtained that damps the high-frequency motions, in a similar way as the Matsuno scheme, but needs somewhat less computer time and, with the same damping intensity, has a higher accuracy for low-frequency meteorologically significant motions.

Using the described method, a 4-day experimental forecast has been made, starting with a stationary Haurwitz-Neamtan solution, for a primitive equation, global, and homogeneous model. The final geopotential height map showed no visible phase errors and only a modest accumulation of truncation errors and effects of numerical smoothing mechanisms. Two shorter experiments have also been made to analyze the effects of space resolution and damping in the process of time differencing. It is felt that the experimental results strongly encourage further testing and investigation of the proposed method.

CONTENTS

1. Introduction and formulation of the method.....	15
2. Space differencing.....	16
3. Time differencing: three-level extrapolation scheme.....	18
4. Remaining details of the method.....	21
Suppression of the space noise.....	21
Trajectory computations.....	22
Transformation of the velocity and acceleration components.....	22
5. Initial conditions.....	22
6. Results of the experiments.....	24
7. Concluding remarks.....	27
Acknowledgments.....	28
References.....	28

1. INTRODUCTION AND FORMULATION OF THE METHOD

Ever since the beginning of the development of modern meteorology, Lagrangean methods have had a strong appeal to theoretical meteorologists. The laws of motion and thermodynamics relate the forces and heating to the individual derivatives of velocity components and po-

tential temperature; and in this way, the Lagrangean approach is the most fundamental one. Nevertheless, due to practical reasons, during the last two decades of extensive research in numerical prediction and atmospheric general circulation experimentation, the Eulerian method of formulating and solving the relevant atmospheric equations has been used almost exclusively. There has been only a modest number of attempts to use a Lagrangean or a quasi-Lagrangean technique. Graphical forecasting methods are essentially Lagrangean (Fjørtoft 1952, 1955); however, their use has diminished with the easier availability of fast digital computers. An example in the paper by Welander (1955) illustrates the major difficulty to be expected in trying to perform a numerical forecast with the use of the classical Lagrangean approach: a chessboard set of fluid elements soon deforms into a highly irregular pattern, unsuitable for space differentiation along the originally straight material lines. Thus, frequent redefinition of the material coordinate lines would be necessary. Besides, the computational complexity of this approach appears to be considerable; see, for example, the analysis by Wiin-Nielsen (1959).

To avoid these problems or for other reasons, a number of investigators have used the Lagrangean formulation of

¹ UCLA Department of Meteorology Contribution No. 180

² Present affiliation: Department of Meteorology, University of Belgrade, Yugoslavia

the advection terms only (Økland 1962, Krishnamurti 1962, Leith 1965). In this way, an advective change at a space-fixed grid point and in a particular time step is essentially obtained by finding the location of the parcel that will in this time step be carried by the flow to the grid point and by computing the corresponding individual value through space interpolation. Since by this procedure a space interpolated value is advected at each grid point and time step, it is not clear whether the method has any Lagrangean-type advantages. It does represent a simple possibility to avoid the "nonlinear" computational instability; however, it is questionable whether the gain in simplicity, as compared to the more involved application of the Arakawa (1966) concept of maintaining the integral constraints of physical importance, will often be of more value than the advantages of the latter alternative. In fact, it has likely been to a rather large extent due to the wide application of the Arakawa conservation schemes that the remarkable achievements in atmospheric simulation experiments have been accomplished in recent years. Besides, other less refined possibilities to overcome the nonlinear instability problem also exist.

Despite this outstanding performance of the present day Eulerian methods, they do contain a number of intrinsic deficiencies. It appears convenient to mention them briefly:

No attempt can be made to conserve, within advection terms, individual properties following the motion of air particles. That is, a false dispersion of the wave components of the flow is produced by the finite-difference formulation of the advection terms (Wurtele 1961, Matsuno 1966b). The error in phase speed of individual waves increases catastrophically when the wavelength approaches the smallest possible wavelength resolvable by the grid. This precludes the formation of sharp gradients of an advected quantity, such as the gradients observed in frontal and intertropical convergence zones, and smooths out these zones in case that some initially exist. Another consequence of the Eulerian formulation of advection terms is that the mentioned process of elongation, tangling, and subsequent mixing of fluid elements is not realistically simulated (Djurić 1966).

It seems futile in Eulerian methods to try alleviating this wave dispersion difficulty by having a higher grid resolution in zones of sharp gradients. These zones are usually moving and after some time would so leave the regions of high resolution. Besides, a space discontinuity in grid resolution results in false reflection of waves at the boundary separating the two regions.

The task of defining the locations of grid points on spherical earth so as to accomplish a quasi-homogeneous space resolution, though feasible in a number of straight-forward ways, is an uncomfortable one, leading to laborious computational schemes (Kurihara and Holloway 1967, Sadoury et al. 1968).

A Eulerian model accepts information at predetermined grid-point locations only, while the observations are and will be made at relatively randomly spaced points. This restriction may be of some disadvantage, especially when, as expected, a crucial part of the atmospheric observations becomes continuous in time.

In trying to remedy the leading of the mentioned shortcomings, it was proposed by Charney (1966) to let the grid points move, as if imbedded in some hypothetical medium, in such a way that the grid spacing constantly adjusts to the gradient of the quantity one wishes to

resolve. In this way, one would have two simultaneous flows: the physical flow of the fluid and the flow of this hypothetical medium. Charney rejected the possibility of allowing the two fluids to coincide since, as described already, the grid lines moving with the physical flow would soon become highly distorted and useless for the computation of space derivatives. It is suggested here to try the other alternative: let the computation points move with the physical fluid and, instead, reject the requirement for the continuity of their relative position. The necessary space derivatives have then to be computed by using the values of the variables at all the computation points that at the particular moment happen to be in some way surrounding the point for which the computation is done. Even if they initially are not, after some time, say a number of days, these surrounding points will be distributed essentially at random; it is conceivable that this may result in a significant increase in the number of computation points necessary to achieve some required accuracy in space differencing. But, in return, the prognostic equations reduce to a set of ordinary, instead of partial, differential equations, with a considerable gain in simplicity. Besides, no errors are produced by the finite-difference treatment of the advection terms since there are no advection terms.

The proposed method has been tested using a global primitive equations model for a homogeneous and incompressible atmosphere. Following sections describe the technical details of the computational procedure as well as the results of a number of performed experiments. Finally, a comparison of the properties of the method with those of the conventional Eulerian schemes will be given.

2. SPACE DIFFERENCING

Throughout this study, we shall deal with a homogeneous, incompressible, and frictionless atmospheric model. Although simple, such a model contains a significant part of the essential features of the large-scale atmospheric motions; see, for example, the discussion in the paper by Arakawa (1970). For these reasons, it has been used many times to test the performance of the numerical finite-difference schemes. The most recent reference describing such a use is probably the one by Grammelvedt (1969); it contains a number of the previous ones. As is customary, the pressure change with height is assumed in the present study to be given by the hydrostatic equation. The pressure force is then not a function of height; and if the initial wind is independent of height, it will have to remain so. We shall assume this to be the case. We shall further consider earth to be a perfect sphere and choose a λ, θ, r spherical coordinate system with, for later convenience, an arbitrary orientation of the $\theta = \pm \pi/2$ axis. Having a shallow atmosphere, we replace the radius r with a constant value a_0 and accordingly (Phillips 1966) neglect the vertical velocity terms in the equations of horizontal motion. The governing equations

then become

$$\frac{dU}{dt} = -\frac{1}{a_e \cos \theta} \frac{\partial \phi}{\partial \Lambda} + 2\Omega V \sin \varphi + \frac{UV}{a_e} \tan \theta,$$

$$\frac{dV}{dt} = -\frac{1}{a_e} \frac{\partial \phi}{\partial \theta} - 2\Omega U \sin \varphi - \frac{U^2}{a_e} \tan \theta,$$

and

$$\frac{d\phi}{dt} = -\phi \left(\frac{1}{a_e \cos \theta} \frac{\partial U}{\partial \Lambda} + \frac{1}{a_e} \frac{\partial V}{\partial \theta} - \frac{V}{a_e} \tan \theta \right). \quad (1)$$

Here, U and V are the horizontal velocity components in the directions of constant θ and constant Λ , respectively; ϕ is the geopotential of the free surface; t is time; time derivatives are individual rates of change, following the motion of the fluid; Ω is the magnitude of the earth's angular velocity; and φ is latitude. We shall further use λ for longitude and denote by u and v the eastward and northward components of the horizontal velocity, respectively.

The problem of space differencing now consists of computing the four space derivatives in eq (1). We want to do this by making use of the known values of u , v , and ϕ at the point for which the computation should be performed, which we shall call the "reference point," and of the values of these variables at a number of surrounding computation points, which we shall call "neighbors." The space distribution of these points is considered to be arbitrary, except for assuming that they are not organized in some special inconvenient way (along a line, for instance). This distribution is given by the known values of their geographical coordinates λ , φ . For a defined orientation of the Λ , θ system, the components u , v and coordinates λ , φ can be transformed readily, of course, into components U , V and coordinates Λ , θ , if this definition is such as to make this necessary.

Now, we may expect that the property of being a neighbor has to be a reciprocal one. If it were not, we would have a situation in which the values of dependent variables at a computation point affect the time change of those at another one, without the opposite being true. It would appear that this should lead to an instability of the computation; indeed, some test runs support this conclusion. The simplest way of making the property of being a neighbor reciprocal is to take as neighbors all the computation points which at that particular moment happen to be within some prescribed distance ρ of the considered reference point; this possibility has been used in the present study. Now, a method for the computation of space derivatives will always require a certain minimal number of neighbors; to make sure that we always have at least that many neighbors in a computation with a randomlike distribution of points, we then have to make ρ such that the average number of neighbors is considerably greater than this minimal one. In this situation, the

method of least squares offers a straightforward way to compute the space derivatives, and it has been used here.

The accuracy of the least-squares fitting, if performed in terms of the geographical coordinates λ , φ , would obviously break down when approaching the two Poles. For avoiding this, the least-squares fitting was done in the coordinate system Λ , θ , which had its origin always in the considered reference point, and $\theta = \pm \pi/2$ axis in its meridional plane, with θ increasing northward. This choice of origin has an additional benefit of simplifying eq (1), in that the three $\tan \theta$ terms disappear, if computed forward in space.

The necessary coordinate transformation equations can be written in the form

$$\Lambda = \arctan(Y/X) \quad (2)$$

and

$$\theta = \arctan(Z/\sqrt{X^2 + Y^2})$$

where

$$X = \cos \varphi_0 \cos \varphi \cos(\lambda - \lambda_0) + \sin \varphi_0 \sin \varphi,$$

$$Y = \cos \varphi \sin(\lambda - \lambda_0),$$

$$Z = -\sin \varphi_0 \cos \varphi \cos(\lambda - \lambda_0) + \cos \varphi_0 \sin \varphi,$$

and λ_0 , φ_0 are the geographical coordinates of the reference point. Except along the meridian through the reference point, the coordinate lines of the Λ , θ system, in general, make an angle with respect to those of the λ , φ system. Denoting this angle by β and having it increase in the positive direction, we obtain from eq (2)

$$\sin \beta = -\sin \varphi_0 \sin(\lambda - \lambda_0) / \sqrt{X^2 + Y^2} \quad (3)$$

and

$$\cos \beta = [\cos \varphi_0 \cos \varphi + \sin \varphi_0 \sin \varphi \cos(\lambda - \lambda_0)] / \sqrt{X^2 + Y^2}.$$

The velocity components U , V can then be computed making use of the relations

$$U = u \cos \beta + v \sin \beta \quad (4)$$

and

$$V = -u \sin \beta + v \cos \beta.$$

After having in this way performed the transformation of coordinates λ , φ and components u , v into coordinates Λ , θ and components U , V , the least-squares fitting was done in the experiments reported here by defining

$$\hat{\chi} = \chi_0 + A_x \Lambda + B_x \theta + C_x \Lambda^2 + D_x \Lambda \theta + E_x \theta^2. \quad (5)$$

Here, χ stands for any of the variables, U , V , and ϕ , and

χ_0 is the value of χ at the reference point; the five coefficients are computed so as to make $\hat{\chi}$ differ as little as possible, in the least-squares sense, from the values of χ at the individual neighbors. Having, as described, more than five neighbors, the two will have to be, in general, different. If we wish, we can prescribe some weights w to the squared differences at the individual neighbors and compute the coefficients so as to minimize the sum

$$S = \sum_{i=1}^n w_i (\chi_i - \hat{\chi}_i)^2. \quad (6)$$

The subscripts here refer to the values of the variables at particular neighbors, the total number of neighbors being n . In the experiments that will be described here, the same weight has been prescribed always to all the neighbors. It might be possible, however, to optimize the weights of individual neighbors in some way, say as a function of their space distribution or the reliability of the χ values at particular neighbors.

Now, obviously, we assume

$$\frac{\partial \phi}{\partial \Lambda} = A_\phi, \quad \frac{\partial \phi}{\partial \theta} = B_\phi, \quad \frac{\partial U}{\partial \Lambda} = A_U, \quad \text{and} \quad \frac{\partial V}{\partial \theta} = B_V; \quad (7)$$

the computation of space derivatives in eq (1) is in this way defined.

A few words could be added about the choice of the neighbor-defining distance ρ and the search for neighbors. Preliminary experiments with the present method have shown that a tendency for the appearance of computational noise exists, this tendency becoming catastrophic with the decrease in ρ . This noise may be partly a result of the constant change of neighbors; this change must be associated with some disruption of the balance in the fields. Another source of the noise should be expected in the errors in space differencing that are produced by inconvenient space distribution of the neighbors. For keeping this noise tendency at an acceptably low level, it was found necessary to have a fairly large average number of neighbors, \bar{n} . The experiments reported here have all been done with the value of

$$\rho = a_e \arccos \left(1 - 2 \frac{\bar{n}}{N} \right) \quad (8)$$

such as to make \bar{n} equal to 30; here, N is the total number of computation points. With such a large value for \bar{n} , no need was felt to check whether the particular values of n are, at each reference point and time step, always greater than or equal to 5.

For enabling a fast search for the neighbors, the globe was divided into spherical grid boxes; and at the beginning of the computation and after each displacement of the computation points, lists of addresses have been made of all the points found in particular boxes. For a specific

reference point, then only the points found in boxes that are within the distance ρ of the reference point have been checked for the possibility of being neighbors. This procedure appeared to be fairly fast, in the sense that it did not consume a major portion of the total computation time.

3. TIME DIFFERENCING: THREE-LEVEL EXTRAPOLATION SCHEME

It has earlier been pointed out by Matsuno (1966a) that a discontinuity in the grid size of a Eulerian grid can result in a false generation of high-frequency waves. As pointed out, this apparently takes place also in our case of an irregular distribution of computation points. For such situations, Matsuno recommended use of a computational scheme that filters out high-frequency oscillations during the process of time integration. His first-order accuracy scheme (Matsuno scheme) has since been used extensively in some of the general circulation studies (Mintz 1965, Arakawa et al. 1969). It was pointed out by Lilly (1965) that this scheme may possibly cause a considerable loss in the energy of the system; on the other hand, for the purpose of initialization for the primitive equations model, some authors felt the need for a scheme with even more powerful damping of the high-frequency motions (Nitta 1969). Use of such high-frequency damping schemes is likely to become much more extensive with the expected advent of the time-continuous observations: we may then wish to use these schemes to speed the adjustment of the imbalances introduced by continuous input of the data into a numerical forecast. In view of this general interest and possible advantage in having a variable-damping scheme, a scheme that was analyzed for use in the present model and can have a variable damping will be described here in more detail. This is the scheme obtained by performing a linear time extrapolation of computed time derivatives to a time value of $t_0 + a\Delta t$ where t_0 is the value of time at the beginning of the considered time step Δt and a is a parameter that we can use to control the properties of the scheme.

We shall write a particular one out of eq (1) in the general form

$$\frac{dx}{dt} = f(x, t), \quad x = x(t). \quad (9)$$

In writing this, we have disregarded the coupling within the system (1) in exchange for the possibility of considering x to be complex and thus having eq (9) stand for a pair of eq (1). If we now use an integer subscript to denote the number of time steps elapsed, we can write the considered finite-difference version of eq (9) as

$$\frac{x_{r+1} - x_r}{\Delta t} = (1+a)f_r - af_{r-1}. \quad (10)$$

For brevity, we shall sometimes call approximation (10)

TLE (three-level extrapolation) scheme. It reduces to the Euler (forward) scheme when $a=0$ and to the simplified Adams-Bashforth scheme when $a=1/2$. When $a=1$, it represents a simulation of the backward difference scheme.

If we define as the truncation error ϵ of the considered scheme, the remainder on the right side of eq (10) when $x_{\tau+1}$ and $f_{\tau-1}$ are substituted by their true values obtained through Taylor series expansion, we have

$$\epsilon = -(\frac{1}{2}-a)f'_r(\Delta t)^2 - \frac{1}{2}(\frac{1}{3}+a)f''_r(\Delta t)^3 + \dots$$

Thus, approximation (10) is of first-order accuracy, unless $a=1/2$, when its accuracy is of the second order.

To analyze the behavior of the error over a period of time, however, we have to prescribe first the function $f(x, t)$. It is of particular interest to consider the case of the oscillation equation

$$\frac{dx}{dt} = i\omega x \tag{11}$$

since it describes the linearized gravity-inertial motions present within eq (1). We shall do so throughout the remainder of this section.

We tentatively write our finite-difference solution of eq (11) in the form

$$x_\tau = x_0 \lambda^\tau. \tag{12}$$

Combining eq (10-12), we then see that eq (12) is the required finite-difference solution of eq (11), provided that

$$\lambda = \frac{1}{2}[1 \pm \frac{1}{2}(A+B)^{1/2}] + i\frac{1}{2}[(1+a)p \pm \frac{1-a}{2|1-a|}(-A+B)^{1/2}] \tag{13}$$

where

$$p = \omega\Delta t,$$

$$A = \frac{1}{2}[1 - (1+a)^2 p^2],$$

and

$$B = \frac{1}{2}[1 + 2(1-6a+a^2)p^2 + (1+a)^4 p^4]^{1/2}.$$

In eq (13), the upper signs correspond to the "physical," and the lower correspond to the spurious "computational mode" that appears through the use of the three time levels differencing scheme. Now, we can also write

$$\lambda = |\lambda| e^{i\theta}. \tag{14}$$

Since the true solution of eq (11) can be written as

$$x(\tau\Delta t) = x_0 e^{i\omega\tau\Delta t},$$

we see it appropriate to refer, as customary, to $|\lambda|$ as the amplification factor and to $\theta/\omega\Delta t$ as the relative phase change (per time step) of the finite-difference solution. For stability, it is now necessary to have both values of $|\lambda| \leq 1$; for accuracy, it is desirable to have $|\lambda|$ and $\theta/\omega\Delta t$

of the physical mode close to unity and to have $|\lambda|$ of the computational mode as small as possible.

We shall first investigate the stability and damping properties of the considered TLE scheme. From eq (13), we obtain

$$|\lambda| = \frac{1}{2}[1 + (1+a)^2 p^2 + B \pm (A+B)^{1/2} \pm \frac{1-a^2}{|1-a|} p(-A+B)^{1/2}]^{1/2}. \tag{15}$$

The right side of eq (15) is equal to unity when

$$\omega\Delta t = \frac{1}{a} \left(-\frac{1-2a}{1+2a} \right)^{1/2}. \tag{16}$$

The TLE scheme is, therefore, stable for values of $\omega\Delta t$ equal to or smaller than the right side of eq (16). This right side has its maximum value

$$(\omega\Delta t)_{max} = \sqrt{2(5\sqrt{5}-11)} \approx 0.6006$$

when

$$a = \frac{1}{4}(1 + \sqrt{5}) \approx 0.8090. \tag{17}$$

Thus, as far as the extent of the stability range is concerned, eq (17) gives the optimum value of the parameter a .

Amplification factors given by eq (15) for this optimum stability and three other particular values of a are plotted against $\omega\Delta t$ in figure 1. It demonstrates a favorable damping of the computational mode for values of $a < 1$. However, the computational and physical mode curves meet for the value of $a=1$ and flip over each other for larger values of a , the computational mode thereby becoming unstable and limiting the stability range of $\omega\Delta t$. Still, the stability range decreases rather slowly with the increase in a , and large values of a may thus be useful if an especially powerful damping of the high-frequency motions is desired.

It is of interest to find the location of the minimum value of the greater of the amplification factors since the scheme has the strongest damping at this value of $\omega\Delta t$, and one may wish to choose Δt so as not to exceed this maximum damping $\omega\Delta t$ value. First, for $a < 1$, one finds from

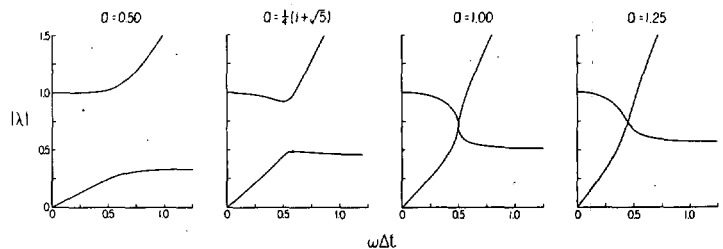


FIGURE 1.—Amplification factors of scheme (10), plotted against $\omega\Delta t$, for values of $a=0.50$ (simplified Adams-Bashforth scheme), $a = \frac{1}{4}(1 + \sqrt{5})$ (value giving the largest stable region of $\omega\Delta t$), $a=1.00$ (a simulated backward scheme), and $a=1.25$.

eq (15) that the two $|\lambda| = \text{constant}$ lines tangent to the $|\lambda|$ curves are

$$|\lambda| = \frac{a^{1/2}}{1+a} [3-a \pm 2^{3/2}(1-a)^{1/2}]^{1/2}. \quad (18)$$

Thus, these are the extreme values of $|\lambda|$, the upper sign again referring to the physical mode. They occur at

$$\omega\Delta t = \frac{1}{(1+a)^2} \times \left[\frac{-17 + 4a - 29a^2 + 2a^3 \mp 2^{5/3}(3-7a+2a^2)(1-a)^{1/2}}{3-2a \pm 2^{3/2}(1-a)^{1/2}} \right]^{1/2}. \quad (19)$$

Hence, for $a < 1$, eq (19) with upper signs gives the maximum damping $\omega\Delta t$ value as a function of a . It has a maximum of about 0.5132 at $a = 1/8$.

For $a > 1$, maximum damping occurs at the intersection of the two $|\lambda|$ curves. This happens at

$$\omega\Delta t = 1/(1+a). \quad (20)$$

Both expressions (19) and (20) are of course valid in the limiting case when $a = 1$.

A summary of the dependence of considered $\omega\Delta t$ values on a is given in figure 2. The figure shows the extent of the stability range, eq (16), and $\omega\Delta t$ values at which the considered TLE scheme has a maximum damping, eq (19) with upper signs for $a \leq 1$ and eq (20) for $a \geq 1$.

To discuss now the accuracy of the finite-difference solution, we also have to consider the phase change, per time step, of its physical mode. Using the subscript 1 to denote the values that pertain to the physical mode, we can write this phase change as

$$\theta_1 = \arctan \left[\left(2(1+a)p + \frac{1-a}{|1-a|} (-A+B)^{1/2} \right) \div (2+(A+B)^{1/2}) \right]. \quad (21)$$

We want to compare θ_1 with the phase change, per time step, of the true solution that is equal to $\omega\Delta t$. For that purpose, ratios of the two phase changes as functions of $\omega\Delta t$ are plotted in figure 3. This is done for a number of values of the parameter a and for comparison also for the first-order Matsuno scheme.

Normally, however, we will only be concerned with the accuracy of the finite-difference solution for small values of $\omega\Delta t$. Thus, we will require $|\lambda_1|$ and $\theta_1/\omega\Delta t$ to be as close as possible to unity only when $\omega\Delta t$ is close to zero. Figures 1 and 3, while giving a general description of the behavior of $|\lambda_1|$ and $\theta_1/\omega\Delta t$, are not very helpful in estimating how well this requirement is satisfied. To this end, consideration of their series expansions in terms of powers of $p = \omega\Delta t$ is more convenient; for these, we obtain

$$|\lambda_1| = 1 + \frac{1}{2}(1-2a)p^2 + \dots \quad (22)$$

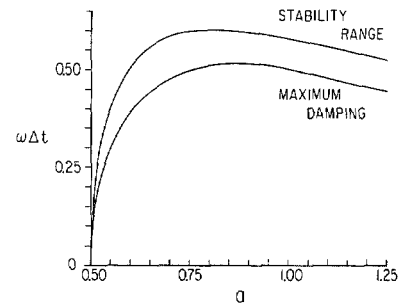


FIGURE 2.—Curves showing the extent of the stability range of scheme (10) and $\omega\Delta t$ values at which a maximum damping occurs as functions of the parameter a .

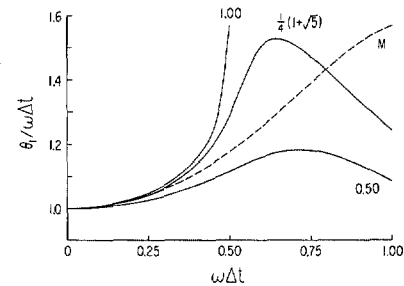


FIGURE 3.—Ratios of the phase changes per time step of finite-difference solutions and the true solution plotted against $\omega\Delta t$. The solid curves refer to the physical mode of scheme (10) and values of the parameter a written by the curves; the dashed curve refers to the first-order Matsuno scheme.

and

$$\theta_1/p = 1 - \frac{1}{3}(1-6a+3a^2)p^2 + \dots \quad (23)$$

Thus, the amplitude error has a minimum in case of the Adams-Bashforth scheme when $a = 1/2$. The phase error, on the other hand, has a minimum when

$$a = 1 \pm \frac{1}{3}\sqrt{6} \approx 1 \pm 0.8165 \quad (24)$$

and a maximum in case of the simulated backward scheme when $a = 1$.

An appropriate estimate of the accuracy of the TLE scheme appears to be its comparison with the first-order Matsuno scheme. The amplitude and relative phase change expansions for this Matsuno scheme are

$$|\lambda_M| = 1 - \frac{1}{2}p^2 + \dots$$

and

$$\theta_M/p = 1 + \frac{2}{3}p^2 + \dots$$

As could have been expected, these leading terms are equal to the values that the corresponding terms in eq (22) and (23) take in case of the simulated backward scheme. We see that, p being the same and small, the amplitude error of the TLE scheme is less than that of the Matsuno scheme for all values of $0 < a < 1$; its phase

error, moreover, is less than the Matsuno scheme error for all reasonable values of a except for $a=1$. Of course, $p=\omega\Delta t$ would not normally be the same; the optimum choice of Δt appears to be such as to obtain maximum damping at the highest expected frequency. Since the minimum amplification factor of the Matsuno scheme, $\sqrt{3}/2 \approx 0.8660$, occurs at $\omega\Delta t=1/\sqrt{2}$, this choice would imply having Δt of the TLE scheme, Δt_{TLE} , shorter than the Δt of the Matsuno scheme, Δt_M , so that

$$\Delta t_{TLE} = \Delta t_M / \sqrt{2}$$

if a is chosen between about 0.7 and 1. Still, since the TLE scheme needs only about half as much computation time per time step as does the Matsuno scheme, computation with the TLE scheme and this choice of time steps would be about 30 percent faster. Having chosen the value of Δt_{TLE} , the intensity of damping of the highest expected frequencies can still be adjusted within fairly wide limits by a suitable choice of a ; the value of $a=1$ would, for instance, result in about two to three times stronger damping of the highest frequencies than with the Matsuno scheme, while the value given by eq (17) would already result in a damping slightly weaker than Matsuno's. At the same time, for low-frequency motions, both amplitude and phase errors of the TLE scheme would be significantly less than the corresponding Matsuno scheme errors. This now includes also the $a=1$ case, since the shortening of the time step leads to an additional decrease in total truncation errors, due to the curved shape of the $|\lambda_1|$ and $\theta_1/\omega\Delta t$ curves.

A possible disadvantage of the present TLE scheme may be its requirement for storage of time derivatives in the computer code of the model. However, in the present floating computation points method, this is offset largely by saving the need for storage of an extra set of point coordinates, what would have been required when using a stable or neutral two-levels scheme.

Use of a three time levels scheme, of course, is associated with a need for a special starting procedure. However, since for reasonable values of a the computational mode of the TLE scheme is strongly damped, no difficulties should be expected if the simplest forward scheme is used for the first time step. This was, therefore, done in the experiments reported here.

Finally, it may be worth mentioning that, obviously, a difference exists between the application of the stability analysis to the present Lagrangean method and its usual application to Eulerian methods. The frequency ω now refers to the individual changes and not to the local changes as in the Eulerian models.

4. REMAINING DETAILS OF THE METHOD

SUPPRESSION OF THE SPACE NOISE

Besides the use of the described high-frequency damping time-differencing scheme, two other noise-suppressing

mechanisms were built into the model. While the purpose of the damping version of the TLE scheme was to suppress the small-scale features in time changes of the dependent variables, the purpose of the remaining two mechanisms was to deal with the apparently more fundamental problem of the growth of the small-scale features in space changes of these variables. This space noise in the fields of dependent variables, as discussed at the end of section 2, appears to be for the most part a result of the accumulation of random truncation errors in space differencing. In Eulerian models, accumulation of such errors is normally prevented by the interaction of the neighboring grid points; each irregularity then behaves as a small-scale gravity-inertial wave and is thus dispersed and possibly also damped in the process of time differencing. This may not be possible in the present method since the space differencing by the least-squares fitting to a large number of neighbors makes the interaction of the neighboring computation points extremely weak—at least when the weight of the neighbors is not made to depend on their distance from the reference point. With the usual mechanism for the suppression of space noise thus mostly lacking, an alternative procedure had to be constructed.

First, a constraint was imposed on the magnitudes of the components of gradients of dependent variables, as computed using the values of the variables at reference points and their nearest neighbors. These magnitudes were not allowed to surpass some arbitrarily prescribed very large values, believed to be impossible in an error-free development of the flow. A check on their actual values was performed at each computation point and time step, before the computation of space derivatives; for the case that this constraint is violated, instructions were provided to change the dependent variables at the two points so as to reduce the gradient component to the allowed magnitude, without changing the average value of the variables. This, in fact, represented an enforcement of the requirement that the dependent variables at two computation points approach each other in case that the distance between these points happens to approach zero. However, the experiments reported here have all been started with initial point distributions such that no two points were close to each other; as a result, only rarely did any two points approach each other very closely, and the described nearest neighbor smoothing most likely, in these experiments, has never been performed.

The second, less exclusive, smoothing mechanism consisted of adding a diffusion simulating term to the right sides of each of the three eq (1). This term had the form

$$-k_d \widehat{(\chi - \chi)} \quad (25)$$

where k_d is a constant and the circumflex represents an average over all the neighbors that are within some prescribed distance ρ_d of the reference point, this distance being less than the distance ρ defined by eq (8). In present

experiments, the distance ρ_d was defined so as to cover an area equal to one-third the area covered by the neighborhood distance ρ , and the constant k_d was defined so as to give unity if multiplied by the time step of 4 hr. The effect of the terms in (25) is expected to be mostly smoothing of the space irregularities in the χ fields that are formed by the individual values of χ . Computation of the χ changes due to the terms in (25) was not done by using the TLE time-differencing scheme, but rather with simple forward steps.

TRAJECTORY COMPUTATIONS

The most straightforward approach to the computation of trajectories of computation points is to consider that it consists of solving the system of equations

$$\begin{aligned} a_e \cos \varphi \frac{d\lambda}{dt} &= u(\lambda, \varphi, t), \\ a_e \frac{d\varphi}{dt} &= v(\lambda, \varphi, t). \end{aligned} \quad (26)$$

It has previously been shown (Djurić 1961, Mesinger 1965) that the truncation errors of trajectory computations are rather small, even with time steps of the order of 1 hr or more. The present method might have high demands with respect to the accuracy of the trajectories; however, since maintenance of linear stability requires much shorter time steps, it appears that even the demands for an extremely high accuracy of the trajectories should be satisfied with any reasonable scheme. One problem, though, is to avoid the polar singularities in eq (26). In computations on a limited domain, this has customarily been accomplished by transforming eq (26) into its counterpart on the image surface of a conformal projection. This seems to be impractical in a global model since no single conformal projection can be used for the entire sphere. However, a simple alternative exists and has been used here: trajectories can be computed using spherical geometry, assuming that each trajectory segment is an arc of a great circle. This procedure is especially comfortable in the present prognostic calculation where it involves no space translation of the velocity vector.

To display the necessary formulas, let us first observe that the displacement of the trajectory points is centered in time if performed using the wind vector

$$\mathbf{v}_{\tau+\frac{1}{2}} = \mathbf{v}_\tau + \frac{1}{2} \frac{d\mathbf{v}}{dt} \Delta t.$$

Here, $d\mathbf{v}/dt$ is the time-extrapolated value of the acceleration as described in the previous section. The angular displacement of a trajectory point in the time step Δt is then

$$\alpha = |\mathbf{v}_{\tau+\frac{1}{2}}| \Delta t / a_e.$$

We now consider the spherical triangle with two of its vertices at the positions of this trajectory point at time

levels τ and $\tau+1$ and with the third vertex at the South Pole. We denote its interior angle at the initial position of this point by γ ; then

$$\cos \gamma = -v_{\tau+\frac{1}{2}} / |\mathbf{v}_{\tau+\frac{1}{2}}|.$$

Using the law of cosines for a spherical triangle, we can now write

$$\begin{aligned} \sin \varphi_{\tau+1} &= \cos \alpha \sin \varphi_\tau - \sin \alpha \cos \varphi_\tau \cos \gamma \\ \text{and} \\ \cos |\Delta \lambda| &= (\cos \alpha - \sin \varphi_{\tau+1} \sin \varphi_\tau) / (\cos \varphi_{\tau+1} \cos \varphi_\tau). \end{aligned} \quad (27)$$

With the addition of the obvious relation

$$\lambda_{\tau+1} = \lambda_\tau + u_{\tau+\frac{1}{2}} |\Delta \lambda| / |u_{\tau+\frac{1}{2}}|, \quad 3 \text{ if } u_{\tau+\frac{1}{2}} \neq 0,$$

the displayed formulas define, in general, the computation of the $\tau+1$ time level coordinates of the considered point. When $u_{\tau+\frac{1}{2}}=0$, the considered triangle collapses into a line, but the first eq (27) is still valid; the second eq (27) is not needed in that case. Finally, another special case of a trajectory point coming exactly to one of the Poles, or to its extreme vicinity, might be harmful; this was avoided by moving the point slightly away from the Pole should such a case tend to occur.

TRANSFORMATION OF THE VELOCITY AND ACCELERATION COMPONENTS

When a computation point is moved to its new $\tau+1$ time level position, its velocity components, the extrapolated acceleration contributions already added, have to be transformed to the new orientation of the geographical λ, φ coordinate lines. Since a one-step displacement is relatively small, we assume no change in the orientation of the Λ, θ coordinate lines. (This is equivalent to forward computation of the small $\tan \theta$ terms in eq (1). One could, of course, compute their space-centered values if desired.) We can then compute the new u, v velocity components by using eq (2), (3), and

$$u = U \cos \beta - V \sin \beta, \quad (28)$$

and

$$v = U \sin \beta + V \cos \beta.$$

Parallel to this, transformation of the nonextrapolated acceleration components also has to be performed so that they can be used for time extrapolation of the acceleration components at the $\tau+1$ time level position of the considered point. This transformation is, of course, done in the same way as the velocity components transformation, except for the acceleration components replacing the corresponding velocity components in eq (28).

5. INITIAL CONDITIONS

A number of test computations were done with the

initial conditions similar to those used by Phillips (1959) and Krishnamurti (1962). They are given by the stream function

$$\psi = -a_e^2 \sin \varphi (k_1 - k_2 \cos^R \varphi \cos R\lambda) \quad (29)$$

where k_1 and k_2 are constants and R (integer) is the wave number. As shown by Haurwitz (1940) for the linearized case and by Neamtan (1946) for the nonlinear one, the flow pattern given by eq (29) will in a nondivergent barotropic atmosphere move from west to east without change of shape and with the angular velocity

$$\nu = \frac{R(3+R)k_1 - 2\Omega}{(1+R)(2+R)} \quad (30)$$

Having a primitive equations model, we need as initial conditions the initial velocity components and height of the free surface. The velocity components equivalent to eq (29) are obtained by

$$u = -\frac{1}{a_e} \frac{\partial \psi}{\partial \varphi} \quad (31)$$

and

$$v = \frac{1}{a_e \cos \varphi} \frac{\partial \psi}{\partial \lambda}$$

The height field associated with eq (29) can be determined by solving the balance equation; as given by Phillips (1959), one obtains

$$\phi = \phi_0 + a_e^2 [A(\varphi) + B(\varphi) \cos R\lambda + C(\varphi) \cos 2R\lambda] \quad (32)$$

where

$$A(\varphi) = \frac{1}{2k_1} (2\Omega + k_1)c^2 + \frac{1}{4}k_2^2 c^{2R} [(R+1)c^2 + (2R^2 - R - 2) - 2R^2 c^{-2}],$$

$$B(\varphi) = \frac{2(\Omega + k_1)k_2}{(R+1)(R+2)} c^R [(R^2 + 2R + 2) - (R+1)^2 c^2],$$

$$C(\varphi) = \frac{1}{4}k_2^2 c^{2R} [(R+1)c^2 - (R+2)],$$

and

$$c = \cos \varphi.$$

It has been pointed out by Phillips that eq (29-32) will also be a solution of the corresponding divergent primitive equations system only if the constant k_1 happens to be such that the wave is stationary. This will occur when

$$k_1 = 2\Omega / [R(3+R)]. \quad (33)$$

If this is not so, the solution of the primitive equations system is unknown. Thus, it appears that the best test of the performance of a barotropic numerical primitive equations model can be made by choosing eq (33) for the definition of k_1 as originally done by Charney (1955). Then we know that any departures of the numerical

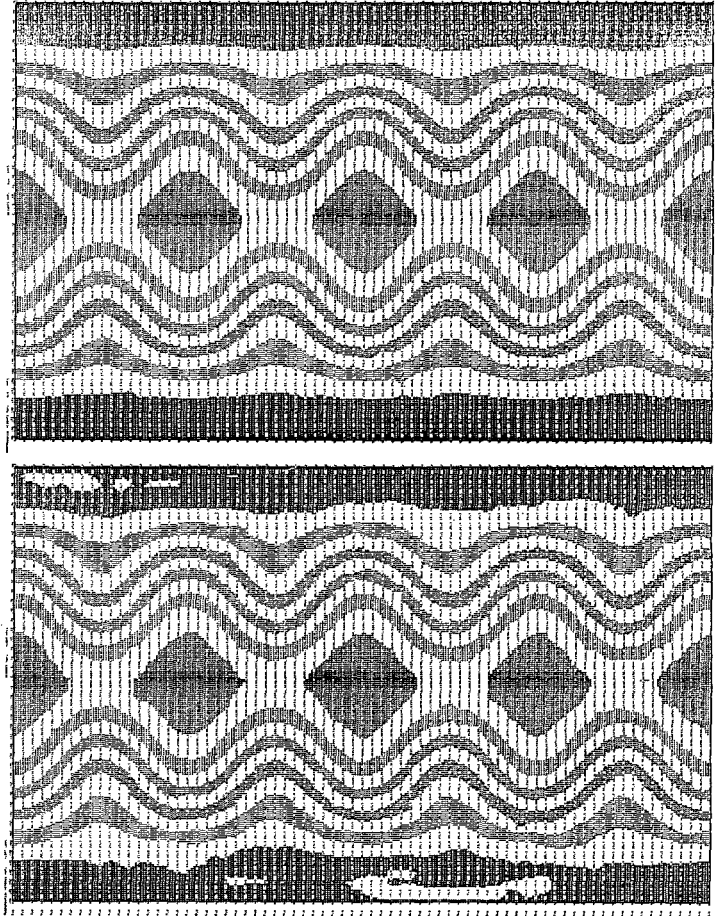


FIGURE 4.—Distribution of the height of the free surface at the beginning (upper map) and at the end (lower map) of the 4-day forecast, shown on a cylindrical meridionally equidistant projection. The maps are printed with a shading interval of 160 gpm.

solution from the initial fields of eq (29), (31), and (32) represent numerical errors. Hence, k_1 was here defined by eq (33); the constants R and ϕ_0 were given the same values as those by Phillips and Krishnamurti, that is,

$$R = 4 \text{ and } \phi_0 = 9.8 \times 8000 \text{ m}^2 \text{ s}^{-2},$$

while the constant k_2 was defined at about half of their value, that is,

$$k_2 = 3.646 \times 10^{-8} \text{ s}^{-1} (= 0.05 \Omega),$$

to obtain velocities more comparable to those observed in the atmosphere. The initial distribution of ϕ , obtained with these values of the constants, is shown in the upper part of figure 4. The initial distributions of u and v are similar to those shown in the paper by Krishnamurti, with u values approximately equal to half of those displayed in his figure 7 and v values, since they do not depend on k_1 , equal to almost exactly half of his values in figure 8.

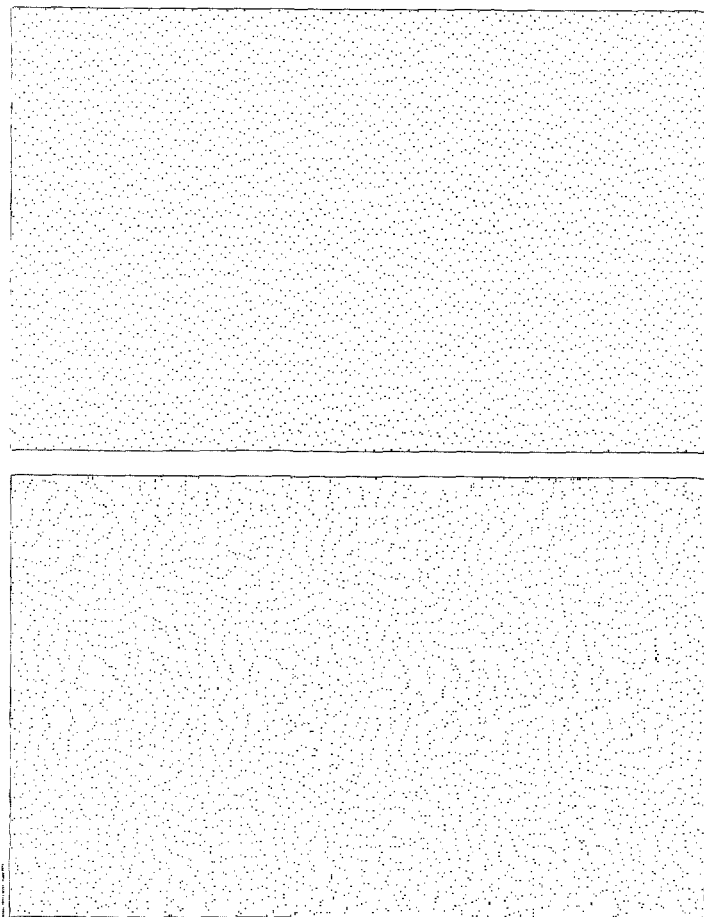


FIGURE 5.—Space distribution of the computation points at the beginning (upper map) and at the end (lower map) of the 4-day forecast, shown on a cylindrical equal-area projection. The projection is conformal at latitudes of about 45° .

The present method, as defined in sections 2 to 4, involves no special choice of the initial space distribution of computation points, as long as each computation point has a sufficient initial number of neighbors. Thus, an initial space distribution of computation points also has to be prescribed. This was done by choosing a distribution between the random and the hexagonal one. Such quasi-hexagonal initial distribution of computation points was accomplished by placing the points at constant increments in longitude and at random on every second of $2L$ equal intervals of the sine of latitude, going repeatedly K times from the South Pole to the North Pole in a chessboard fashion (placing the points at successive sweeps on odd and on even of the $2L$ intervals). Computation points then form an irregular $K \times L$ point grid on an equal-area cylindrical projection of the globe with consecutive somewhat slanted columns of points shifted relative to one another so as to form a quasi-hexagonal pattern. A particular space distribution of 160×25 points obtained in this way is shown as the upper part of figure 5; it was used for the 4000-point experiments presented here.

6. RESULTS OF THE EXPERIMENTS

A 4-day forecast was computed using the described method and initial conditions. It was made with 4000 computation points, time steps of 12 min, and time extrapolation parameter a equal to the value of $0.25(1 + \sqrt{5})$, which accomplishes the maximum stability range of Δt . Values of the remaining numerical constants have already been given in the preceding sections. Besides this 4-day experiment, two shorter 1-day runs have been performed: one differing from the 4-day run only in having a coarser space resolution of 3000 points arranged initially in a 120×25 point grid and the other only in having the parameter a equal to $\frac{1}{2}$, that is, by being computed using the Adams-Bashforth time-differencing scheme.

Results of the 4-day experiment will be illustrated here by a number of maps and diagrams. As first of these, figure 4 shows in its lower part the geopotential field at the end of the 4-day period; it can be compared with the initial field shown in the upper map, both on a cylindrical meridionally equidistant projection. These maps were obtained by performing a space interpolation of the geopotential values to points of the spherical 72×46 point grid (5° by 4° in longitude and latitude) and then using a usual mapping program with a 160 gpm contour interval. The space interpolation was done by finding always three nearest computation points to a particular spherical grid point and then fitting a linear polynomial to the geopotential values at these three points—with an additional constraint that the interpolated value must remain within the range between the lowest and the highest of the considered geopotential values. This constraint had the purpose of protecting against an unfavorable space distribution of the three nearest points when they are organized nearly along a line; otherwise, a meaningless result could be obtained in such a case. A slight amount of noise can be introduced occasionally into the maps by such interpolation as can be seen by close inspection of the upper map showing the initial field that contained no noise in the computation points data. An alternative interpolation procedure would be to perform a least-squares fitting to the values at the four nearest computation points; in that way, a smoothing effect would be obtained.

An outstanding feature of the 4-day map is the fact that no phase errors can be noticed: locations of the trough and ridge lines appear to be exactly the same as on the initial map. The amount of noise present, despite all precautions, may seem somewhat discouraging. However, most of it appears in polar regions where the geopotential field was initially rather flat, with the lowest 8000 gpm isolines running along the polar lines of the projection. Thus, only a small occasional decrease in the geopotential heights was sufficient to produce noise in the map shading in these regions; moreover, this noise is shown on the map with exaggerated space dimensions due to the large area magni-

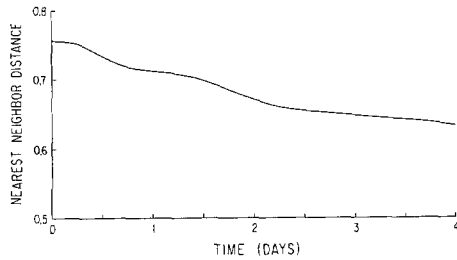


FIGURE 6.—Mean value of the distances from each computation point to its nearest neighbor as a function of time for the 4-day experiment.

fication in the vicinity of a Pole. In other words, the unfavorable visual impression as to the amount of noise present in the final geopotential field is to some extent deceiving. A fair amount of noise can be seen along the Equator where the field is also flat; but the remaining contour lines in regions of stronger gradients are often remarkably smooth.

In figure 5, the initial (upper map) and final (lower map) space distribution of computation points is shown on an equal-area cylindrical projection so as to reflect their number per unit area of the globe. One can notice that, in the 4-day map, the points exhibit a tendency to organize along irregular lines; this must be a consequence of the fact that, except for some noise, no turbulence was present in the computed flow fields. A more irregular final distribution of points should of course be expected when the points are advected by a less organized flow.

Starting with an initial distribution of points that is better than random, one must expect it to deteriorate with time and eventually become random or possibly worse than random—"better" and "worse" meaning that the points are more and less evenly dispersed than in a random distribution, respectively. In fact, some earlier experiments (Mesinger 1965) have shown that the nondivergent part of an observed two-dimensional atmospheric flow had the property of producing as well as maintaining a random distribution of initially organized and floating particles while divergent flows maintained distributions worse than random in the above sense. The time rate of this process is of interest and will be discussed here along with its effect on the accuracy of the forecast.

For giving a statistical description of the distribution of our computation points, it is convenient to consider the mean distance from each point to its nearest neighbor. It has been shown by Hertz (1909) that, when a very large number of points is distributed at random on a plane and the unit of length chosen so as to make their average concentration equal to 1, this mean distance will be equal to 0.5. If, however, the points are distributed at random only relative to one another but with a concentration that is a function of space, this mean distance has to be less than the random distribution value of 0.5 (Mesinger

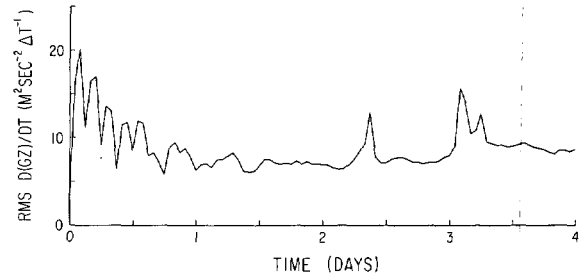


FIGURE 7.—Root-mean-square individual change per time step in the geopotential height as a function of time. The values refer to the 4-day experiment.

1965). Finally, if the points are organized relative to one another, this mean distance can of course be greater; it is, for example, equal to $\sqrt{2}/4\sqrt{3} \approx 1.0746$ when the points are arranged into a hexagonal grid. Apparently when the mean nearest neighbor distance is greater, we might expect a better performance of a particular distribution of computation points. This mean distance was computed at 1-hr intervals in the 4-day experiment: its initial value, corresponding to the distribution shown in the upper map of figure 5, was equal to about 0.7555; it decreased rather slowly later on, reaching a value of about 0.6319 at the end of the experiment. The obtained mean distances as a function of time are shown in figure 6. It can be compared with figure 7 in the aforementioned paper by the author; in that previous experiment, the nondivergent part of an observed flow needed much less time, only about half a day, to accomplish the same decrease in the mean nearest neighbor distance. The difference, again, is due to the lack of turbulence in the present experiment.

For obtaining a more quantitative idea of the amount of various kinds of noise present in the 4-day experiment, a record of the root-mean-square (rms) individual change per time step in the geopotential heights is shown in figure 7—also based on computations at 1-hr intervals. Computed per unit time and divided by the rms value of the geopotential height, this quantity would give the mass-weighted rms value of $\text{div}(\text{divergence}) \mathbf{v}$. Thus, it is equal to zero in the analytic solution and does not depend on time.

In the experiment, the initial value of the rms individual geopotential change was equal to about $3.38 \text{ m}^2 \text{ s}^{-2}/12 \text{ min}$; this corresponds to the value of about $0.5 \times 10^{-7} \text{ s}^{-1}$ for the mentioned value of $\text{div} \mathbf{v}$. Compared with the Pole-to-Equator change in the free-surface height of somewhat more than 1600 gpm, this initial error of about $1/3 \text{ gpm}/12 \text{ min}$ appears to be moderate; in fact, some caution should be exercised here since these numbers may already be influenced by the round-off error of the performed IBM single precision computations. Since there is no noise in the initial fields, this error—assuming no round-off influence—reflects only the difference be-

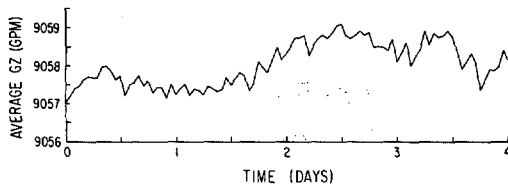


FIGURE 8.—Average height of the free surface as a function of time for the 4-day experiment.

tween the analytic space derivatives of velocity components and those computed by the least-squares fitting of a second-degree polynomial to the values at available neighbors. Thus, it shows a combined effect of the inconvenient space distribution and number of neighbors and of the truncation of higher order terms in the polynomial. Some feeling for the relative significance of these two factors can of course be obtained through suitable experiments. For instance, the 3000-point run, with points arranged into a 120×25 pattern, had this initial error equal to $3.97 \text{ m}^2 \text{ s}^{-2}/12 \text{ min}$; this must have been mostly a consequence of the increased importance of the neglected higher order terms. On the other hand, a different organization of the 4000 points into a 100×40 instead of 160×25 pattern with a 0.7997 mean nearest neighbor distance was found to result in a reduction of this error to the value of 2.75 of the same units.

During the first day or so, the considered quantity is seen to undergo vigorous gravity-type oscillations with a period of very nearly 3 hr. These oscillations must be set off by small systematic differences between the analytic and computed space derivatives. By the end of about 1 day, the oscillations are damped out through the process of time differencing. The parallel run, differing from the 4-day run only by being computed with the Adams-Bashforth time-differencing scheme, did not exhibit such damping; and the oscillations persisted without noticeable change in amplitude throughout the 1-day period of the experiment.

At times after about 1 day, the rms individual geopotential change seen in figure 7 settles at the value of about twice the initial one, showing the contribution of the random space noise in the velocity fields. After about 2 days, a slow rise in this rms change can be noticed, interrupted by three irregular sudden increases. The gradual rise in this quantity should probably be attributed to the slow deterioration of the space dispersion of computation points, and the three peaks to occasional occurrences of very inconvenient configurations of neighbors.

Performance of the model can further be analyzed by examination of the behavior of global integrals of a number of relevant physical quantities. Conservation of none of these integrals is formally guaranteed in the present method, and a change in conservative quantities thus reflects the effect of numerical errors or of the artificial

smoothing mechanisms. A record of one of such quantities, the average height of the free surface, is shown in figure 8, again based on values computed at 1-hr intervals. This average was obtained by using the geopotential values interpolated to points of the spherical 72×46 point grid, by interpolation described earlier in this section. The interpolation protects the computed average values against the effect of possible systematic variations in the space density of computation points; this protection seems necessary since such variations would be correlated with those in the height of the free surface. The time changes in the average free-surface height shown in figure 8 appear to be random and of a modest amplitude. The observed amplitude of less than 2.1 gpm represents about 0.02 percent of the total average height. The considered average is of course proportional to the total mass of the fluid.

It may be noted that, using eq (32), one can obtain

$$\bar{\phi} = \phi_0 + \frac{a_c^2}{2} \left[\frac{2}{3} k_1 (2\Omega + k_1) - k_2^2 (R+1)(R+2) \frac{2 \cdot 4 \cdot 6 \cdots 2R}{3 \cdot 5 \cdot 7 \cdots (2R+3)} \right] \quad (34)$$

where

$$\bar{\phi} = \frac{1}{4\pi} \int_{-\pi/2}^{\pi/2} \int_0^{2\pi} \phi \cos \varphi \, d\varphi \, d\lambda$$

is the global average value of ϕ . With the values of constants given in section 5, eq (34) gives 9057.33 gpm for the average free-surface height. The initial value of 9057.02 gpm entered in figure 8 happens to be slightly less than this "exact" value, the difference showing the amount of the sampling error. This exact value could also have been entered to start the curve in figure 8, what would have further reduced its amplitude.

Finally, a record of the average values of total, kinetic, and available potential energy computed also at 1-hr intervals is shown in figure 9. Denoting the total kinetic energy averaged per unit mass by K_1 and the available potential energy averaged in the same way by A_1 , we have

$$K_1 = \frac{1}{2} \iint_S \phi \mathbf{v}^2 dS / \iint_S \phi dS \quad (35)$$

and

$$A_1 = \frac{1}{2} \iint_S (\phi - \bar{\phi})^2 dS / \iint_S \phi dS \quad (36)$$

where S represents the total area of the globe. In computing the values of K_1 and A_1 , shown in figure 9, these integrals and global average of ϕ in eq (36) were substituted by corresponding sums and by the average of ϕ based on values of ϕ and \mathbf{v}^2 interpolated again to points of the spherical 72×46 point grid. Thus, the values obtained for K_1 and A_1 were also protected against systematic

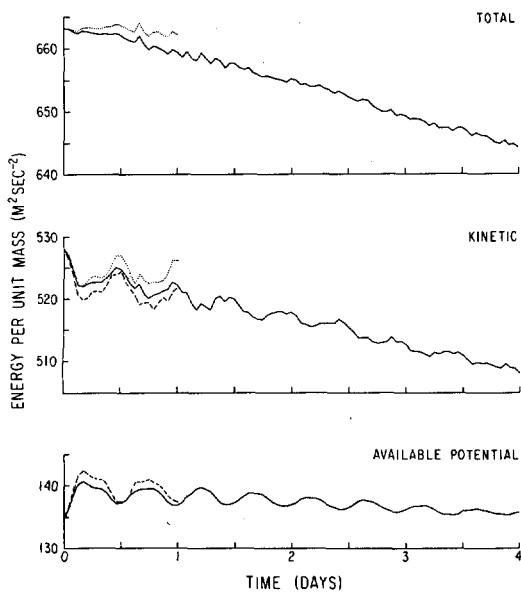


FIGURE 9.—Average values per unit mass of the total, kinetic, and available potential energy as functions of time. The solid curves refer to the 4-day experiment; the dashed curves refer to the parallel 3000-point experiment, differing from the 4-day one only in the number of computation points; and the dotted curves refer to the parallel $a = \frac{1}{2}$ (Adams-Bashforth scheme) experiment, differing from the 4-day one only in the value of this parameter of the time-differencing scheme.

variations in the space density of computation points. Such a protection seems desirable since it appears that there should exist a definite correlation between these variations and those in the contributions to total energy values. However, it is this space interpolation that gives rise to the time noise seen in the kinetic (and thus also total) energy curves in figure 9; no time noise appears when the integrals in eq (35) are computed by taking simple sums of corresponding quantities over all the computation points. Of the energy curves, the solid ones obviously refer to the 4-day experiment; the dashed curves refer to the "coarse resolution" 3000-point run, and the dotted ones to the run performed by using the nondamping Adams-Bashforth time-differencing scheme.

An outstanding characteristic of the energy curves is a periodic exchange between the kinetic and available potential energy. These oscillations are apparently brought forth by the truncation of the higher order terms in the least-squares polynomial. Namely, it would seem that in this way one computes pressure gradients that are predominantly smaller, in their absolute values, than the analytic ones. Since the initial Coriolis forces are not affected by the space-differencing method, an imbalance is obtained such as to set off inertia-gravity oscillations in which the fluid particles initially move predominantly toward higher free-surface heights; this is associated with an increase in available potential and a decrease in kinetic energy. The amplitude of these oscillations should

then increase with an increase in the neighbor-defining distance due to the increased importance of the neglected higher order terms; this is confirmed by the dashed kinetic energy curve. Namely, since the average number of neighbors \bar{n} was the same in all of the three experiments, the neighbor-defining distance of the 3000-point experiment was greater than that of the two 4000-point ones; accordingly, this 3000-point experiment exhibits a greater amplitude of the discussed oscillations. In the 4000-point 4-day experiment, this amplitude initially amounts to about 1.1 percent of the total kinetic energy and decreases later on. Damping in the time differencing and physical dispersion of the waves are responsible for this decrease in amplitude. The period of the oscillations is less than the pure inertial one, in accordance with the usual linear theory; see, for example, the paper by Arakawa (1970).

The energy curves in figure 9 exhibit a general decreasing trend, showing the loss of energy due to the artificial space smoothing and damping in the time differencing. During the 4-day experiment, the total kinetic energy decreases by about 3.71 percent of its initial value. One part of this energy is transformed into the available potential energy through the described inertia-gravity oscillations and subsequent geostrophic adjustment; it somewhat more than compensates for the loss in the latter to the existing space-time smoothing mechanisms, leaving the potential energy at a value slightly higher than the initial one. The remaining part is dissipated through the numerical smoothing processes.

It is tempting to try estimating the relative contributions of space smoothing and time differencing to the observed kinetic energy loss. One may attempt to do this with the help of the results of the parallel run computed using the Adams-Bashforth time-differencing scheme. This run was terminated at the 1-day time; at that moment, its loss in kinetic energy amounts only to somewhat less than one-third of that demonstrated by the solid kinetic energy curve in figure 9. However, some caution should be exercised in interpreting this difference since there is a possibility that it appears partly as a consequence of the weak instability of the Adams-Bashforth scheme. No visual sign of such instability, though, could be noticed by careful comparison of the two 1-day geopotential height maps; thus, a value for the parameter a smaller than the one used for the 4-day experiment appears preferable.

7. CONCLUDING REMARKS

The proposed Lagrangean method offers a number of distinct advantages over the conventional Eulerian technique. We shall summarize them here:

Formulation of the problem involves no advection terms; this makes the governing equations simple, free of nonlinear instability, and guarantees, except for truncation errors, the conservation of

individual properties following the motion of fluid particles. In other words, there is no computational dispersion in the advection terms. This should improve the simulation of mesoscale phenomena, such as fronts, jets, and intertropical convergence zones, associated with sharp gradients of an advected quantity. Further, this enables a realistic simulation of the deformation-dependent process of lateral diffusion.

The simulated flow is not subjected to systematic space changes in grid resolution and properties. With computation points moving with the fluid, a quasi-homogeneous resolution is accomplished without any geometrical considerations.

The two mentioned properties significantly reduce the amount of work needed to code a computer program for the model. Absence of considerations related to the geometry of a particular grid and to the treatment of advection terms relieves the programmer of a major effort that these considerations require in a Eulerian global model.

It would appear easy to accomplish a variable resolution, such as to have a higher density of computation points in regions of rapid spatial change in appropriate quantities. Such regions exhibit a strong tendency to move with the fluid and would thus maintain this increased resolution for an extended time. A density dependent neighbor-defining distance could then be used, while still observing the principle of property of being a neighbor having to be a reciprocal one.

The model can accept information at arbitrary points in space, and they can be prescribed different weights, depending on their reliability. This seems ideally suited to the expected future global observation system (ICSU/IUGG 1967).

On the other hand, a number of objections could be raised:

The present experiments showed a tendency for the appearance of computational noise, and artificial smoothing was needed to suppress this tendency. However, the situation should be better when a simulation of the real atmospheric diffusion is incorporated into the model.

It may be difficult or impossible to construct schemes that would conserve global integrals of relevant quantities.

It seems that more computation time and more points are needed than in a comparable Eulerian model. The 4000-point experiments described here required about 50 min of the IBM 360/91 computer time per 1 day of simulated time.

Finally, some uncertainty remains as to how severe the performed test was; it would appear that a task of maintaining a stationary state, with computation points floating through it, is fairly demanding. Still, one feels a need for a more nonlinear two-dimensional test and of course a three-dimensional one. The amount of effort invested into the present method is exceedingly small compared to that which brought the Eulerian methods to the present state; this, coupled with the results of the present study, would seem to highly encourage further investigation of the proposed method.

ACKNOWLEDGMENTS

The author is grateful to Profs. Yale Mintz and Akio Arakawa for their encouragement of this research and for some helpful suggestions. Messrs. Wayne Schubert and Robert Haney kindly helped to prepare the manuscript by proposing numerous improvements in its text. Computing assistance was obtained from the Campus Computing Network, University of California, Los Angeles.

REFERENCES

- Arakawa, Akio, "Computational Design for Long-Term Numerical Integration of the Equations of Fluid Motion: Two-Dimensional Incompressible Flow, Part I," *Journal of Computational Physics*, Vol. 1, No. 1, July 1966, pp. 119-143.
- Arakawa, Akio, "Numerical Simulation of Large-Scale Atmospheric Motions," *Numerical Solution of Field Problems in Continuum Physics*, American Mathematical Society, Providence, R.I., 1970, pp. 24-40.
- Arakawa, Akio, Katayama, Akira, and Mintz, Yale, "Numerical Simulation of the General Circulation of the Atmosphere," *Proceedings of the WMO/IUGG Symposium on Numerical Weather Prediction, Tokyo, November 26-December 4, 1968*, Japan Meteorological Agency, Tokyo, Mar. 1969, pp. IV-7-IV-12.
- Charney, Jule G., "The Use of the Primitive Equations of Motion in Numerical Prediction," *Tellus*, Vol. 7, No. 1, Feb. 1955, pp. 22-26.
- Charney, Jule G., "Some Remaining Problems in Numerical Weather Prediction," *Advances in Numerical Weather Prediction*, Travelers Research Center, Inc., Hartford, Conn., 1966, pp. 61-70.
- Djurić, Dušan, "On the Accuracy of Air Trajectory Computations," *Journal of Meteorology*, Vol. 18, No. 5, Oct. 1961, pp. 597-605.
- Djurić, Dušan, "The Role of Deformation in the Large-Scale Dispersion of Clusters," *Quarterly Journal of the Royal Meteorological Society*, Vol. 92, No. 392, Apr. 1966, pp. 231-238.
- Fjørtoft, Ragnar, "On a Numerical Method of Integrating the Barotropic Vorticity Equation," *Tellus*, Vol. 4, No. 3, Aug. 1952, pp. 179-194.
- Fjørtoft, Ragnar, "On the Use of Space-Smoothing in Physical Weather Forecasting," *Tellus*, Vol. 7, No. 4, Nov. 1955, pp. 462-480.
- Gammeltvedt, Arne, "A Survey of Finite-Difference Schemes for the Primitive Equations for a Barotropic Fluid," *Monthly Weather Review*, Vol. 97, No. 5, May 1969, pp. 384-404.
- Haurwitz, Bernhard, "The Motion of Atmospheric Disturbances on the Spherical Earth," *Journal of Marine Research*, Vol. 3, 1940, pp. 254-267.
- Hertz, Paul, "Über den gegenseitigen durchschnittlichen Abstand von Punkten, die mit bekannter mittlerer Dichte im Raume angeordnet sind" (On the Average Mutual Distance of Points Distributed in Space With a Known Average Density), *Mathematische Annalen*, Vol. 67, Springer-Verlag, Berlin, 1909, pp. 387-398.
- ICSU/IUGG-Committee on Atmospheric Sciences, *Report of the Study Conference Held at Stockholm, 28 June-11 July 1967, on the Global Atmospheric Research Programme (GARP)*, World Meteorological Organization, Geneva, 1967, 144 pp.
- Krishnamurti, Tiruvalam N., "Numerical Integration of Primitive Equations by a Quasi-Lagrangian Advective Scheme," *Journal of Applied Meteorology*, Vol. 1, No. 4, Dec. 1962, pp. 508-521.
- Kurihara, Yoshio, and Holloway, J. Leith, Jr., "Numerical Integration of a Nine-Level Global Primitive Equations Model Formulated by the Box Method," *Monthly Weather Review*, Vol. 95, No. 8, Aug. 1967, pp. 509-530.
- Leith, Cecil E., "Lagrangian Advection in an Atmospheric Model," *World Meteorological Organization Technical Note No. 66*, Geneva, 1965, pp. 168-176.
- Lilly, Douglas K., "On the Computational Stability of Numerical Solutions of Time-Dependent Non-Linear Geophysical Fluid Dynamics Problems," *Monthly Weather Review*, Vol. 93, No. 1, Jan. 1965, pp. 11-26.
- Matsuno, Taroh, "Numerical Integrations of the Primitive Equations by a Simulated Backward Difference Method," *Journal of the Meteorological Society of Japan*, Ser. II, Vol. 44, No. 1, Feb. 1966a, pp. 76-84.

- Matsuno, Taroh, "False Reflection of Waves at the Boundary Due to the Use of Finite Differences," *Journal of the Meteorological Society of Japan*, Ser. II, Vol. 44, No. 2, Apr. 1966b, pp. 145-157.
- Mesinger, Fedor, "Behavior of a Very Large Number of Constant-Volume Trajectories," *Journal of the Atmospheric Sciences*, Vol. 22, No. 5, Sept. 1965, pp. 479-492.
- Mintz, Yale, "Very Long-Term Global Integration of the Primitive Equations of Atmospheric Motion," *World Meteorological Organization Technical Note No. 66*, Geneva, 1965, pp. 141-167.
- Neamtan, S. M., "The Motion of Harmonic Waves in the Atmosphere," *Journal of Meteorology*, Vol. 3, No. 2, June 1946, pp. 53-56.
- Nitta, Takashi, "Initialization and Analysis for the Primitive Equation Model," *Proceedings of the WMO/IUGG Symposium on Numerical Weather Prediction, Tokyo, November 26-December 4, 1968*, Japan Meteorological Agency, Tokyo, Mar. 1969, pp. VI-11-VI-20.
- Økland, Hans, "An Experiment in Numerical Integration of the Barotropic Equation by a Quasi-Lagrangian Method," *Geofysiske Publikasjoner*, Vol. 22, No. 5, Oslo, Jan. 1962, 10 pp.
- Phillips, Norman A., "Numerical Integration of the Primitive Equations on the Hemisphere," *Monthly Weather Review*, Vol. 87, No. 9, Sept. 1959, pp. 333-345.
- Phillips, Norman A., "The Equations of Motion for a Shallow Rotating Atmosphere and the Traditional Approximation," *Journal of the Atmospheric Sciences*, Vol. 23, No. 5, Sept. 1966, pp. 626-628.
- Sadourny, Robert, Arakawa, Akio, and Mintz, Yale, "Integration of the Nondivergent Barotropic Vorticity Equation With an Icosahedral-Hexagonal Grid for the Sphere," *Monthly Weather Review*, Vol. 96, No. 6, June 1968, 351-356.
- Welander, Pierre, "Studies on the General Development of Motion in a Two-Dimensional, Ideal Fluid," *Tellus*, Vol. 7, No. 2, May 1955, pp. 141-156.
- Wiin-Nielsen, Aksel, "On the Application of Trajectory Methods in Numerical Forecasting," *Tellus*, Vol. 11, No. 2, May 1959, pp. 180-196.
- Wurtele, Morton G., "On the Problem of Truncation Error," *Tellus*, Vol. 13, No. 3, Aug. 1961, pp. 379-391.

[Received March 5, 1970; revised May 6, 1970]

CORRECTION NOTICE

Vol. 98, No. 7, July 1970: p. 531, photo of fig. 3 should be interchanged with photo of fig. 4.